

**Unified Framework for Hybrid Aleatory and Epistemic
Uncertainty Propagation via Decoupled Multi-Probability
Density Evolution Method**

Yi Luo

Institute for Risk and Reliability, Leibniz University Hannover
Callinstraße 34, Hannover, 30167, Germany
Department of Civil and Environmental Engineering, Rice University
6100 Main Street, Houston, 77005, TX, USA
E-mail address: yi.luo@irz.uni-hannover.de

Meng-Ze Lyu*

Department of Civil & Environmental Engineering, Hong Kong University of Science
& Technology
Clear Water Bay, Kowloon, 999077, Hong Kong, China
E-mail address: lyumz@ust.hk

Matteo Broggi

Institute for Risk and Reliability, Leibniz University Hannover
Callinstraße 34, Hannover, 30167, Germany
E-mail address: broggi@irz.uni-hannover.de

Marko Thiele

SCALE GmbH
Levelingstr. 40, Ingolstadt, 85049, Germany
E-mail address: marko.thiele@scale.eu

Vasileios C. Fragkoulis

Department of Civil and Environmental Engineering, University of Liverpool
Liverpool, L69 3GH, UK
E-mail address: vasileios.fragkoulis@liverpool.ac.uk

Michael Beer

Institute for Risk and Reliability, Leibniz University Hannover
Callinstraße 34, Hannover, 30167, Germany
Department of Civil and Environmental Engineering, University of Liverpool
Liverpool, L69 3GH, UK
International Joint Research Center for Resilient Infrastructure & International Joint
Research Center for Engineering Reliability and Stochastic Mechanics, Tongji

University
1239 Siping Road, Shanghai, 200092, China
E-mail address: beer@irz.uni-hannover.de

Abstract:

This paper presents a unified framework for uncertainty propagation in dynamical systems involving hybrid aleatory and epistemic uncertainties. The framework accommodates precise probabilistic, imprecise probabilistic, and non-probabilistic representations, including the distribution-free probability-box (p-box). A central aspect of the framework involves transforming the original uncertainty inputs into an augmented random space, yielding the primary challenge of determining the conditional probability density function (PDF) of the response quantity of interest given epistemic uncertainty parameters. The recently proposed decoupled multi-probability density evolution method (decoupled M-PDEM) is employed to numerically solve the conditional PDF for complex dynamical systems. Several numerical examples illustrate the applicability, efficiency, and accuracy of the proposed framework. These include a linear single-degree-of-freedom (SDOF) system subject to Gaussian white noise with its natural frequency modeled as a p-box, a 10-DOF hysteretic structure subject to imprecise seismic loads, and a crash box model with mixed random and interval system parameters.

Keywords: unified treatment; hybrid aleatory and epistemic uncertainty; distribution-free p-box; decoupled multi-probability density evolution method (decoupled M-PDEM).

1 Introduction

Modern engineering systems encounter a variety of complex uncertainties throughout their service life (Ang & Tang 1984, 2006). The performance of engineering structures—from super-tall buildings resisting intense earthquakes (Lyu et al. 2024a), and long-span bridges enduring strong winds (Wang et al. 2024), to nuclear power plant containments under disastrous loads (Lyu et al. 2024b), and offshore platforms subject to wave loads (Luo et al., 2022)—is significantly influenced by inherent randomness (aleatory uncertainty) in material properties, geometric parameters, boundary conditions, and spatiotemporal variations in external excitations (Li & Chen 2009). These aleatory uncertainties are fundamentally irreducible, and their probabilistic characteristics are typically derived from long-term observational data (Lyu et al. 2025a). Concurrently, epistemic uncertainties, arising from incomplete understanding and inadequate control over complex systems (Li 1996, Möller & Beer 2004), also play a crucial role. Examples include limited sensor placements in structural health monitoring (Papadimitriou 2004), theoretical simplifications in constitutive models for novel materials (Soize 2000), and limitations in understanding multi-field coupling mechanisms (Ni & Jiang 2020, Behrendt et al. 2022). These uncertainties inevitably lead to incorporate subjective judgments and idealized assumptions into engineering models (Lind 1983, Beer et al. 2013). Distinguishing reducible epistemic uncertainty from irreducible aleatory uncertainty is critical for enhancing structural safety and economic efficiency in engineering decision-making (Der Kiureghian & Ditlevsen 2009).

In uncertainty quantification (UQ), aleatory and epistemic uncertainties are typically modeled using distinct frameworks (Faes et al. 2021). For aleatory uncertainty, probabilistic models provide a comprehensive mathematical characterization of through probability distribution functions, covariance structures, stochastic processes, or random fields (Soize 2017). However, traditional probabilistic approaches may

introduce biases when epistemic uncertainty arises due to data scarcity or incomplete knowledge (Ditlevsen 1982, Moens & Vandepitte 2005). Consequently, non-probabilistic models such as interval analysis (Moore et al. 2009, Gao et al. 2010) and fuzzy sets (Zadeh 1965, Yao & Furuta 1986, Wang & Qiao 1993), imprecise probabilistic models including probability boxes (p-boxes) (Ferson et al. 2003), and evidence theory (Toussi & Yao 1982, Helton et al. 2010, Jiang et al. 2013), and hyper-parameter/hierarchical probabilistic models (Sankararaman & Mahadevan 2013, Tao & Chen 2022, Behrendt et al. 2025), have been developed, forming a multi-level toolbox for uncertainty quantification. For instance, interval methods excel when parameter bounds are known but distribution information is lacking (Jiang et al. 2015), while p-boxes provide conservative analyses under small sample sizes by defining bounds on probability distributions (Bi et al. 2019).

Propagation of hybrid aleatory and epistemic uncertainties is a critical scientific challenge requiring synergistic treatment within a unified framework. Conventional double-loop approaches, involving outer loops for epistemic uncertainties and inner loops for aleatory uncertainties, often suffer from prohibitively high computational costs, particularly for large engineering systems (Xiu et al. 2010, Sankararaman & Mahadevan 2011, Liu et al. 2018). Recent developments aim to decouple this nested computational structure using augmented uncertainty spaces. Examples include the extended Monte Carlo simulation (MCS) method combined with importance sampling (Wei et al. 2014) and its enhancement via high-dimensional model representation (HDMR) (Wei et al. 2019a, b), and generalized polynomial chaos expansions (Wang & Ghanem 2021). However, these methods are unsuitable for distribution-free p-box inputs. Alternatively, Faes et al. (2020, 2021) leveraged operator norms of linear systems to decouple uncertainties by first identifying worst-case epistemic parameters. However, this approach remains limited to linear systems, and extensions to weakly nonlinear systems rely on statistical linearization technique (Ni et al. 2022, Jerez et al. 2024). Within the probability density evolution method (PDEM) framework (Chen &

Li 2007), integration with change of probability measure (COM) (Chen & Wan 2019, Wan et al. 2024) has enabled efficient computation in scenarios involving epistemic uncertainty considered by input probability distribution updates (Wan et al. 2020, 2023, Yang et al. 2025). However, its accuracy diminishes for large variation in input distributions, and it lacks universal compatibility across diverse epistemic uncertainty representations (Jiang et al. 2018).

This study introduces a unified framework for propagating epistemic and hybrid uncertainties, leveraging an augmented random space strategy to handle various epistemic uncertainty models, including distribution-free p-boxes. The proposed augmented space strategy transforms the hybrid uncertainty propagation into a unified problem of conditional probability density function (PDF) solution. Specifically, the decoupled multi-probability density evolution method (decoupled M-PDEM) (Lyu et al. 2024d) is employed to efficiently compute high-dimensional joint and conditional PDFs. The decoupled M-PDEM, based on the random event description of the principle of preservation of probability (Li & Chen 2008), decomposes high-dimensional joint PDF solution into sets of manageable one-dimensional partial differential equations, thus overcoming the "curse of dimensionality" and facilitating applications to complex engineering systems with multiple outputs (Lyu et al. 2024c, 2025b, Wan et al. 2025, Xiang et al. 2025).

The remainder of the paper is structured as follows: Section 2 formulates the mathematical problem of hybrid uncertainty propagation, encompassing random variables, probability boxes, and interval models within a generalized propagation framework. Section 3 rigorously derives the decoupled M-PDEM, and introduced its application strategy to hybrid uncertainty propagation. Numerical experiments on representative dynamical systems validate the effectiveness of the proposed approach in Section 4. Finally, Section 5 concludes with a summary and outlines future research directions.

2 Augmented Random Space Treatment for Different Types of Uncertainties

2.1 Preliminary discussions

In this work, the uncertain parameters are categorized into the following three types based on the information they convey.

- 1) Random variables, described by precise probabilistic models, are denoted as θ_R . It is described by a probability distribution with joint cumulative distribution function (CDF) denoted as $F_R(\theta_R)$.
- 2) Imprecise probability parameters. Here take variables modeled by p-box as a representative, denoted as θ_p . For a scalar p-box variable, denoted as X , it is described by a set of distribution functions that adhere to the following constraints (Beer et al. 2013):

$$\underline{F}_X(x) \leq F_X(x) \leq \bar{F}_X(x), \quad (1)$$

$$\int_{-\infty}^{\infty} x dF_X(x) \in m, \quad (2)$$

$$\left(\int_{-\infty}^{\infty} x^2 dF_X(x) \right) - \left(\int_{-\infty}^{\infty} x dF_X(x) \right)^2 \in v, \quad (3)$$

and

$$F_X(x) \in \mathcal{F}. \quad (4)$$

Eqs. (1)-(4) indicate that the CDF falls within the lower and upper bound $\underline{F}_X(x)$ and $\bar{F}_X(x)$; the mean value of X falls within the interval m , and variance is bounded by the interval v ; the distribution belongs to a prescribed admissible distribution set \mathcal{F} . For simplicity, it can be denoted as $\langle \bar{F}_X(x), \underline{F}_X(x), m, v, \mathcal{F} \rangle$.

- 3) Non-probabilistic parameters, here considering interval variables, denoted as θ_I . The system's outputs vary depending on the types and combinations of inputs. Similarly,

the outputs fall into one of the three categories.

- 1) When the inputs consist solely of random variables θ_R , the outputs are also random variables, aligning target problem of classical stochastic dynamic analysis methods, such as the probability density evolution method (PDEM) (Chen et al. 2016, Chen & Wan 2019, Li & Wang 2023).
- 2) If the inputs comprise only non-probabilistic parameters (θ_I), the outputs are non-probabilistic parameters as well. Theoretically speaking, the PDEM can address this by treating interval parameters as random variables with bounded distributions. However, using the PDEM in this context offers no advantage over optimization strategies.
- 3) If the inputs include p-box variables θ_p , or any combinations of the three input types, the outputs will be p-box variables.

This study primarily focuses on the latter scenario, where the outputs are p-box variables. The subsequent discussion will be structured according to the different types of inputs.

2.2 Hybrid random and non-probabilistic inputs

First consider systems with hybrid random and interval variables as inputs. The interval input parameters θ_I has the support $[a, b]$. The corresponding output quantity of interest, denoted as X , would be a p-box parameter. It can be described by CDF set bounded by the lower CDF $\underline{F}_X(x)$ and upper CDF $\bar{F}_X(x)$, i.e., $\underline{F}_X(x) \leq F_X(x) \leq \bar{F}_X(x)$.

The corresponding lower and upper CDF can be given by

$$\underline{F}_X(x) = \min_{\theta_I \in [a, b]} F_{X|\theta_I}(x|\theta_I), \quad (5)$$

and

$$\bar{F}_X(x) = \max_{\theta_I \in [a, b]} F_{X|\theta_I}(x|\theta_I), \quad (6)$$

respectively, where $F_{X|\theta_I}(x|\theta_I)$ is the conditional CDF with respect to interval input

parameters. More strictly, the p-box output is further restricted to the distributed sets given by

$$\mathcal{F} = \langle F_{X|\Theta_I}(x|\theta_I) \rangle, \theta_I \in [a, b]. \quad (7)$$

Therefore, a complete description of the output uncertainty can be given by the p-box $\langle \bar{F}_X(x), \underline{F}_X(x), \mathcal{F} \rangle$.

For system with combined random and fuzzy inputs, the output would be a fuzzy p-box, and the probability information of output can be similarly obtained by changing the support of the input fuzzy variables.

2.3 P-box inputs

Then, consider the p-box types of input θ_p , $F_p(\theta_p) \in \langle \bar{F}_p(\theta_p), \underline{F}_p(\theta_p), m, v, \mathcal{F} \rangle$. No matter distribution-free or parametric, the upper and lower bound of response CDF can all be given by

$$\bar{F}_X(x) = \max \left\{ \int_{-\infty}^x \int_{-\infty}^{\infty} f_{X|\Theta_p}(x|\theta_p) f_p(\theta_p) d\theta_p dx \right\}, \quad (8)$$

and

$$\underline{F}_X(x) = \min \left\{ \int_{-\infty}^x \int_{-\infty}^{\infty} f_{X|\Theta_p}(x|\theta_p) f_p(\theta_p) d\theta_p dx \right\}. \quad (9)$$

In these equations, $f_p(\theta_p)$ is any possible PDF of θ_p . Notice that if only p-box variables are involved in the uncertain inputs, the conditional PDF is a Dirac- δ function as given by

$$f_{X|\Theta_p}(x|\theta_p) = \delta \left[x - X(\Theta_p) \Big|_{\Theta_p = \theta_p} \right]. \quad (10)$$

If random variables θ_r are also involved in the input, the conditional distribution will spread out to a “distribution”.

2.4 General discussion

For all the other combinations of the previously discussed types of uncertain parameters,

the problem can be solved by a simple combination of the above-mentioned procedures. Denote all the epistemic uncertainty parameters involved in the system as θ_E . It can be seen that the most crucial step is to obtain the conditional CDF $F_{X|\theta_E}(x|\theta_E)$ or the conditional PDF $f_{X|\theta_E}(x|\theta_E)$. Normally, a double loop scheme need be applied to obtain it. Whereas, by assigning a pseudo distribution to the epistemic parameters, which can be represented by the PDF function $\tilde{f}_{\theta_E}(\theta_E)$, the conditional distribution can be further obtained by

$$f_{X|\theta_E}(x|\theta_E) = \frac{\tilde{f}_{X\theta_E}(x, \theta_E)}{\tilde{f}_{\theta_E}(\theta_E)}. \quad (11)$$

In this equation, the pseudo joint PDF $\tilde{f}_{X\theta_E}(x, \theta_E)$ is probable to be solved via single-loop schemes. In the next section, the recently developed decoupled M-PDEM ([Lyu et al. 2024d](#)) will be implemented.

3 Solution via Decoupled M-PDEM

In this section, the theoretical foundation and the numerical implementation of the decoupled M-PDEM ([Lyu et al. 2024d](#)) will be introduced. It is developed to efficiently solve the joint PDF of the responses of dynamical systems. However, in the current status, the systems considered involves solely aleatory uncertainty, i.e., random variables, as input.

3.1 Theoretical foundation

Consider an n -dimensional dynamical system given by the equation of motion as

$$\dot{X}(t) = g[X(t), \Theta, t], \quad (12)$$

where $X(t)$ is the n -dimensional response process, and $\dot{X}(t)$ is its time-derivative; Θ denotes the random source of the system and is an s -dimensional random variable; $g(\cdot)$

is an n -dimensional deterministic function vector.

Suppose $\mathbf{Z}(t)$ is the m -dimensional response quantity of interest. The generalized density evolution equation (GDDE), or named as the Li-Chen equation (Nielsen et al. 2016), of the joint PDF of $\mathbf{Z}(t)$ and $\boldsymbol{\Theta}$, denoted as $p_{\mathbf{Z}\boldsymbol{\Theta}}(\mathbf{z}, \boldsymbol{\theta}, t)$, can be given by (Li & Chen 2008, Chen & Li 2009)

$$\frac{\partial p_{\mathbf{Z}\boldsymbol{\Theta}}(\mathbf{z}, \boldsymbol{\theta}, t)}{\partial t} + \sum_{i=1}^m \dot{h}_i(\boldsymbol{\theta}, t) \frac{\partial p_{\mathbf{Z}\boldsymbol{\Theta}}(\mathbf{z}, \boldsymbol{\theta}, t)}{\partial z_i} = 0. \quad (13)$$

where $h_i(\boldsymbol{\theta}, t)$ is the component of the solution of $\mathbf{Z}(t) = \mathbf{h}(\boldsymbol{\theta}, t) = [h_1(\boldsymbol{\theta}, t), \dots, h_m(\boldsymbol{\theta}, t)]^T$, and $\dot{h}_i(\boldsymbol{\theta}, t)$ is its derivative with respect to time. The formal analytical solution of Eq. (13) can be given by

$$p_{\mathbf{Z}\boldsymbol{\Theta}}(\mathbf{z}, \boldsymbol{\theta}, t) = p_{\boldsymbol{\Theta}}(\boldsymbol{\theta}) \prod_{i=1}^m \delta[z_i - h_i(\boldsymbol{\theta}, t)] \quad (14)$$

Notice that if only one component of $\mathbf{Z}(t)$, i.e., $Z_i(t)$, is considered, its corresponding Li-Chen equation can be given as

$$\frac{\partial p_{Z_i\boldsymbol{\Theta}}(z_i, \boldsymbol{\theta}, t)}{\partial t} + \dot{h}_i(\boldsymbol{\theta}, t) \frac{\partial p_{Z_i\boldsymbol{\Theta}}(z_i, \boldsymbol{\theta}, t)}{\partial z_i} = 0. \quad (15)$$

The analytical solution is

$$p_{Z_i\boldsymbol{\Theta}}(z_i, \boldsymbol{\theta}, t) = p_{\boldsymbol{\Theta}}(\boldsymbol{\theta}) \delta[z_i - h_i(\boldsymbol{\theta}, t)]. \quad (16)$$

Comparing Eq. (14) with Eq. (16), one has (Lyu et al. 2024d)

$$p_{\mathbf{Z}\boldsymbol{\Theta}}(\mathbf{z}, \boldsymbol{\theta}, t) = \frac{1}{[p_{\boldsymbol{\Theta}}(\boldsymbol{\theta})]^{m-1}} \prod_{i=1}^m p_{Z_i\boldsymbol{\Theta}}(z_i, \boldsymbol{\theta}, t). \quad (17)$$

Eq. (17) indicates that the m -dimensional Li-Chen equation given by Eq. (13) can be analytically treated by solving m decoupled one-dimensional Li-Chen equation given by Eq. (15), which is the key concept of decoupled M-PDEM. Finally, the joint PDF of $\mathbf{Z}(t)$, denoted as $p_{\mathbf{Z}}(\mathbf{z}, t)$, can be given by

$$p_{\mathbf{Z}}(\mathbf{z}, t) = \int_{\mathbb{R}^s} p_{\mathbf{Z}\boldsymbol{\Theta}}(\mathbf{z}, \boldsymbol{\theta}, t) d\boldsymbol{\theta}. \quad (18)$$

3.2 Numerical implementation

The numerical implementation of decoupled M-PDEM follows the basic steps of numerical realization of the PDEM, but with an additional step in between to assemble the marginal PDF into joint PDF. Specifically, it follows five steps.

Step 1. Partitioning the probability space of random input. This further includes the following processes. (1) Generating n_{sel} representative samples of input variables Θ , denoted as $\theta^{(q)}$, $q=1,2,\dots,n_{\text{sel}}$. (2) Partitioning the assigned probability domain $\Omega^{(q)}$ of each point $\theta^{(q)}$ based on the Voronoi diagram, and calculating the assigned probability, which is given by

$$P^{(q)} = \int_{\Omega^{(q)}} p_{\Theta}(\theta) d\theta. \quad (19)$$

Numerically, the integration can be computed by MCS. (3) Reformulation of the point set based on generalized F-discrepancy (Chen & Zhang 2013), obtain the final value of $\theta^{(q)}$.

Step 2. Representative deterministic analysis. That is, for each representative point $\theta^{(q)}$, solve Eq. (12), and obtain $\mathbf{Z}^{(q)}(t) = \mathbf{h}(\theta^{(q)}, t)$.

Step 3. Solving the Li-Chen equation. For each dimension of $\mathbf{Z}(t)$ and for each $\theta^{(q)}$, substitute $\dot{h}_i(\theta, t) \approx \dot{h}_i(\theta^{(q)}, t)$ into the corresponding Li-Chen equation [Eq. (15)] and integral on θ within the subdomain $\Omega^{(q)}$. It yields

$$\frac{\partial p_{Z_i}^{(q)}(z_i, t)}{\partial t} + \dot{h}_i(\theta^{(q)}, t) \frac{\partial p_{Z_i}^{(q)}(z_i, t)}{\partial z_i} = 0, \text{ for } i=1, \dots, m, \text{ and } q=1, \dots, n_{\text{sel}} \quad (20)$$

where

$$p_{Z_i}^{(q)}(z_i, t) = \int_{\Omega^{(q)}} p_{Z, \Theta}(z_i, \theta, t) p_{\Theta}(\theta) d\theta \approx p_{Z, \Theta}(z_i, t | \theta^{(q)}) P^{(q)}. \quad (21)$$

The initial condition for Eq. (20) can be cast as

$$p_{Z_i}^{(q)}(z_i, t) = \delta[z_i - Z_i^{(q)}(0)] P^{(q)}. \quad (22)$$

Eq. (20) can be solved by various numerical schemes, such as the finite difference scheme (Li & Chen 2004) or the mesh free scheme (Wang et al. 2021). Herein, the path

integration is used for the solution.

Step 4. Assembling the joint PDF for each representative point. The sub-joint-PDF of $\mathbf{Z}(t)$ corresponding to the probability sub-domain $\Omega^{(q)}$ can be computed as

$$p_{\mathbf{Z}}^{(q)}(\mathbf{z}, t) = \frac{1}{[P^{(q)}]^{m-1}} \prod_{i=1}^m p_{Z_i}^{(q)}(z_i, t), \text{ for } q = 1, \dots, n_{\text{sel}}. \quad (23)$$

Step 5. Integrating the joint PDF. $p_{\mathbf{Z}}(\mathbf{z}, t)$ is calculated by

$$p_{\mathbf{Z}}(\mathbf{z}, t) = \sum_{i=1}^{n_{\text{sel}}} p_{\mathbf{Z}}^{(q)}(\mathbf{z}, t). \quad (24)$$

It should be noted that another significant advantage of the decoupled M-PDEM scheme lies in the storage of high-dimensional joint PDF. For an m -dimensional random variable, suppose each dimension is discretized into n_i grid points, where $i = 1, \dots, m$. Then, size of the joint PDF would be $\prod_{i=1}^m n_i$. However, via the decoupled M-PDEM scheme, the probability information of the joint PDF is distributed into each representative point with each dimension decoupled. Consequently, the size for storing it would be $n_{\text{sel}} \sum_{i=1}^m n_i$. With the increasing of m , $n_{\text{sel}} \sum_{i=1}^m n_i \ll \prod_{i=1}^m n_i$.

The decoupled M-PDEM can be further collaborated with any variance reduction (Bittner et al. 2024) and adaptive sampling schemes (Zhou et al. 2019), similarly as for PDEM, to improve its efficiency and accuracy. However, it is out of the scope of this work, and is not discussed herein.

3.3 Decoupled M-PDEM for epistemic/hybrid uncertainty propagation

In order to get the solution of $\tilde{f}_{X\Theta_E}(x, \theta_E)$ in Eq. (11) via the decoupled M-PDEM, one can create a response process vector as

$$\mathbf{Z}(t) = [X(t), \tilde{\Theta}_E(t)]^T, \quad t \in [0, \bar{T}] \quad (25)$$

where \bar{T} is the duration of simulated response process $X(t)$; $\tilde{\Theta}_E(t)$ is the pseudo stochastic process associated with the epistemic uncertainty input parameter, and can be simply defined as a linear process as

$$\tilde{\Theta}_E(t) = \frac{t}{T} \Theta_E, \quad t \in [0, \bar{T}]. \quad (26)$$

By solving the joint PDF of $\mathbf{Z}(t)$, we could obtain that $p_Z(\mathbf{z}, t) = \tilde{f}_{X|\Theta_E}(x(T), \theta_E)$.

Substitute it into Eq. (11), the condition PDF $f_{X|\Theta_E}(x(T)|\theta_E)$ can be obtained.

4 Numerical Examples

4.1 SDOF linear systems subject to Gaussian white noise

Consider a single-degree-of-freedom (SDOF) oscillator given by the equation of motion as

$$\ddot{X}(t) + 2\zeta\omega\dot{X}(t) + \omega^2 X(t) = \xi(t), \quad (27)$$

where $X(t)$, $\dot{X}(t)$, and $\ddot{X}(t)$ denotes the displacement, velocity, and acceleration of the oscillator, respectively; ζ denotes the damping ratio; ω denotes the natural frequency; $\xi(t)$ is a Gaussian white noise that satisfies $E[\xi(t)] = 0$, $E[\xi(t)\xi(t+\tau)] = 2\pi S_0 \delta(\tau)$. In this system, the natural frequency ω is considered as a p-box variable, defined by $\omega \sim \langle \bar{F}_\Omega(\omega), \underline{F}_\Omega(\omega) \rangle$, $\omega > 0$. Two response statistics are considered as outputs.

The first is the steady-state variance of $X(t)$, denoted as Y_1 , which is quantified by the p-box $Y_1 \sim \langle \bar{F}_{Y_1}(y_1), \underline{F}_{Y_1}(y_1) \rangle$. Given $\Omega = \omega$, its analytical solution is $y_1 = \frac{\pi S_0}{2\zeta\omega^3}$.

Subsequently, since the determination of Y_1 only involves p-box input, according to Eq.

(10), one has $f_{Y_1|\Omega}(y_1|\omega) = \delta\left(y_1 - \frac{\pi S_0}{2\zeta\omega^3}\right)$, and $F_{Y_1}(y_1) = 1 - F_{\Omega}(\omega) \Big|_{\omega = \left(\frac{\pi S_0}{2\zeta y_1}\right)^{1/3}}$. Further, due to

the monotonicity of Y_1 with respect to ω , based on Eqs. (8) and (9), the upper and lower bounds of the CDF of Y_1 can be analytically given as

$$\begin{cases} \bar{F}_{Y_1}(y_1) = 1 - \bar{F}_{\Omega}[\omega(y_1)] \\ \underline{F}_{Y_1}(y_1) = 1 - \underline{F}_{\Omega}[\omega(y_1)] \end{cases}. \quad (28)$$

The second is the steady-state of $X(t)$. It is denoted as Y_2 , and quantified by the p-box $Y_2 \sim \langle \bar{F}_{Y_2}(y_1), \underline{F}_{Y_2}(y_1) \rangle$. The uncertainty quantification of Y_2 involves both random variables (Gaussian white noise) and p-box variable as inputs. If ω is given, the steady state of $X(t)$ follows the Gaussian distribution, with zero-mean, and variance equals to Y_1 . That is,

$$f_{Y_2|\Omega}(y_2|\omega) = \frac{1}{\sqrt{2\pi y_1}} \exp\left[-\frac{y_2^2}{2y_1}\right], \quad y_1 = \frac{\pi S_0}{2\zeta\omega^3}. \quad (29)$$

Further,

$$F_{Y_2}(y_2) = \int_{-\infty}^{y_2} \int_0^{\infty} \phi\left(\frac{\tilde{y}_2}{\sqrt{y_1}}\right) f_{Y_1}(y_1) dy_1 d\tilde{y}_2 = \int_0^{\infty} \Phi\left(\frac{\tilde{y}_2}{\sqrt{y_1}}\right) f_{Y_1}(y_1) dy_1, \quad (30)$$

where $\phi(\cdot)$ and $\Phi(\cdot)$ denote the PDF and CDF of standard Gaussian variable,

respectively. Notice that $\Phi\left(\frac{\tilde{y}_2}{\sqrt{y_1}}\right)$ is piecewise monotonic with respect to y_1 . Namely,

for $\tilde{y}_2 < 0$, the value of $\Phi\left(\frac{\tilde{y}_2}{\sqrt{y_1}}\right)$ increase with the increasing of y_1 ; for $\tilde{y}_2 > 0$,

$\Phi\left(\frac{\tilde{y}_2}{\sqrt{y_1}}\right)$ decrease with the increasing of y_1 . In this regard, the analytical solution of the

upper and lower bounds of the CDF of Y_2 can be derived as

$$\bar{F}_{Y_2}(y_2) = \begin{cases} \int_0^\infty \Phi\left(\sqrt{\frac{2\zeta\omega^3}{\pi S_0}} y_2\right) \bar{f}_\Omega(\omega) d\omega, & y_2 < 0 \\ 1/2, & y_2 = 0 \\ \int_0^\infty \Phi\left(\sqrt{\frac{2\zeta\omega^3}{\pi S_0}} y_2\right) \underline{f}_\Omega(\omega) d\omega, & y_2 > 0 \end{cases}, \quad (31)$$

and

$$\underline{F}_{Y_2}(y_2) = \begin{cases} \int_0^\infty \Phi\left(\sqrt{\frac{2\zeta\omega^3}{\pi S_0}} y_2\right) \underline{f}_\Omega(\omega) d\omega, & y_2 < 0 \\ 1/2, & y_2 = 0 \\ \int_0^\infty \Phi\left(\sqrt{\frac{2\zeta\omega^3}{\pi S_0}} y_2\right) \bar{f}_\Omega(\omega) d\omega, & y_2 > 0 \end{cases}, \quad (32)$$

respectively.

The analytical solutions [Eqs. (28), (31), and (32)] of Y_1 and Y_2 are derived directly based on the framework proposed in Section 2 without any numerical treatment. Only the upper and lower bounds of the natural frequency ω is employed, and thus illustrate the effectiveness of the proposed augmented random space scheme. These analytical solutions can be utilized to validate the numerical solution by the decoupled M-PDEM. In the numerical example, take $S_0 = 1$, $\zeta = 0.05$, and

$$\bar{F}_\Omega(\omega) = \begin{cases} \Phi\left(\frac{\omega - \mu_1}{\sigma_2}\right), & \omega \leq \mu_1 \\ \Phi\left(\frac{\omega - \mu_1}{\sigma_1}\right), & \omega > \mu_1 \end{cases}, \quad \underline{F}_\Omega(\omega) = \begin{cases} \Phi\left(\frac{\omega - \mu_2}{\sigma_1}\right), & \omega \leq \mu_2 \\ \Phi\left(\frac{\omega - \mu_2}{\sigma_2}\right), & \omega > \mu_2 \end{cases}, \quad (33)$$

where $\mu_1 = 1.9$, $\mu_2 = 2.1$, $\sigma_1 = 0.1$, and $\sigma_2 = 0.2$.

Fig. 1 shows the comparison of the analytical solution of Y_1 given by Eq. (28) and the corresponding numerical solution obtained by the decoupled M-PDEM based on 200, 400, and 800 samples. It can be seen that the decoupled M-PDEM solution converge quickly to the analytical on with the increasing number of samples, and can reach high very high accuracy with the merely 800 samples used.

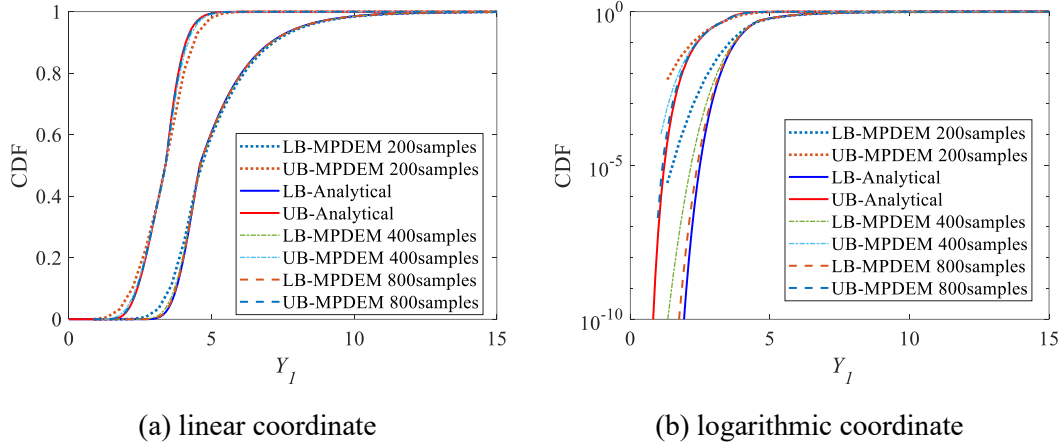


Fig. 1 Upper bounds (UB) and lower bounds (LB) of the CDF of Y_I obtained by analytical solution and decoupled M-PDEM with various sample sizes.

Fig. 2 juxtaposes the analytical solutions and decoupled M-PDEM solutions for Y_2 , which shows great agreement. Notice that in the numerical simulation of the decoupled M-PDEM, only ω is sampled, and the analytical conditional PDF given by Eq. (29) is substituted into the **step 3** of the numerical procedure of decoupled M-PDEM as the solution of Li-Chen equation for $X(t)$. This treatment naturally inserts analytically known information into the numerical implementation of decoupled M-PDEM, and greatly improves the accuracy. That is why, in this case, with only 200 samples, the decoupled M-PDEM solution can show such high accuracy.

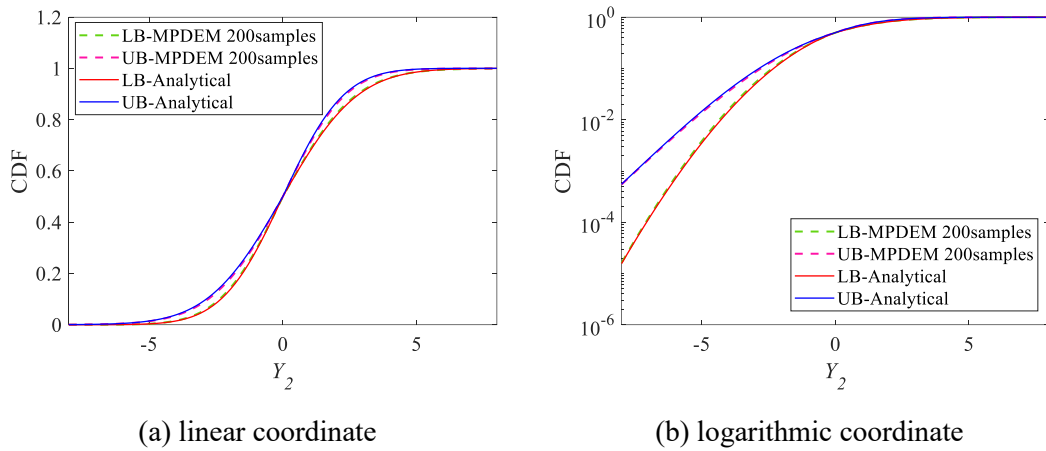


Fig. 2 Upper bounds (UB) and lower bounds (LB) of the CDF of Y_2 obtained by analytical solution and decoupled M-PDEM

4.2 10-DOF Bouc-Wen oscillator subject to imprecise excitation

This example demonstrates the application of the proposed framework to systems subject to excitations characterized by imprecise power spectral density (IPSD). Such problems are typically complex, necessitating a double-loop procedure; however, the proposed framework effectively decouples this complexity.

Consider a 10-DOF system with Bouc-Wen hysteretic model. The equation of motion is given by

$$\mathbf{M}(\boldsymbol{\Theta})\ddot{\mathbf{X}}(t) + \mathbf{C}(\boldsymbol{\Theta})\dot{\mathbf{X}}(t) + \mathbf{f}[\mathbf{X}(t), \mathbf{Z}(t), \boldsymbol{\Theta}] = \mathbf{B}\xi_I(t). \quad (34)$$

where $\mathbf{X}(t)$, $\dot{\mathbf{X}}(t)$, and $\ddot{\mathbf{X}}(t)$, respectively, denotes the displacement, velocity, and acceleration; $\boldsymbol{\Theta} = [\theta_1, \theta_2, \dots, \theta_{20}]^T$ is the vector of random parameters; $\mathbf{M} = \text{diag}[m_1\theta_1, m_2\theta_1, \dots, m_{10}\theta_{10}]$ is the diagonal mass matrix; $\mathbf{C} = a_0\mathbf{M} + a_1\mathbf{K}$ is the linear damping matrix in which

$$\mathbf{K} = \begin{bmatrix} k_1\theta_{11} + k_2\theta_{12} & -k_2\theta_{12} & & & & \\ & -k_2\theta_{12} & k_2\theta_{12} + k_3\theta_{13} & -k_3\theta_{13} & & \\ & & \ddots & \ddots & \ddots & \\ & & & -k_9\theta_{19} & k_9\theta_{19} + k_{10}\theta_{20} & -k_{10}\theta_{20} \\ & & & & -k_{10}\theta_{20} & k_{10}\theta_{20} \end{bmatrix}, \quad (35)$$

and

$$\begin{pmatrix} a_0 \\ a_1 \end{pmatrix} = \frac{2\zeta}{\omega_1 + \omega_3} \begin{Bmatrix} \omega_1\omega_3 \\ 1 \end{Bmatrix}; \quad (36)$$

ω_1 and ω_3 are respectively the square root of the first and third minimum eigenvalue of $\mathbf{M}^{-1}\mathbf{K}$; and ζ denotes the damping ratio. $\mathbf{Z}(t) = [Z_1, Z_2, \dots, Z_{10}]^T$ denotes the vector of the inter-story hysteretic components, and the restoring force is given by

$$\mathbf{f}[\mathbf{X}(t), \mathbf{Z}(t)] = [f_1^* - f_2^*, f_2^* - f_3^*, \dots, f_{n-1}^* - f_n^*, f_n^*]^T, \quad (37)$$

and

$$f_j^*[\mathbf{X}(t), \mathbf{Z}(t)] = k_j [\varepsilon X_j^* + (1 - \varepsilon) Z_j], j = 1, \dots, n, \quad (38)$$

in which $\mathbf{X}^* = [X_1, X_2 - X_1, \dots, X_n - X_{n-1}]^T$ denotes the vector of inter-story drift.

The evolution of the inter-story hysteretic component Z_j satisfies (Ma et al. 2004)

$$\begin{aligned}\dot{Z}_j(t) &= g(\dot{X}_j^*, Z_j, \varepsilon_j) \\ &= \frac{h(\dot{X}_j^*, Z_j, \varepsilon_j)}{1 + \delta_\eta \varepsilon_j} \left[A \dot{X}_j^* - (1 + \delta_v \varepsilon_j) (\beta |\dot{X}_j^*| Z_j + \gamma \dot{X}_j^* |Z_j|) \right].\end{aligned}\quad (39)$$

In this equation, δ_η is the stiffness degradation parameter; δ_v is the strength degradation parameter; A , β , and γ are the parameters for basic hysteresis shape control; ε_j is proportional to the dissipated energy through hysteresis, which is given by

$$\varepsilon_j(t) = \int_0^t \dot{X}_j^*(\tau) Z_j(\tau) d\tau. \quad (40)$$

In Eq. (39), $h(\dot{X}_j^*, Z_j, \varepsilon_j)$ is a pinching shape function, which takes the form

$$h(\dot{X}_j^*, Z_j, \varepsilon_j) = 1 - \zeta_1 \exp \left\{ - \left[Z_j \operatorname{sgn}(\dot{X}_j^*) - q Z_{j,u} \right]^2 / \zeta_2^2 \right\}, \quad (41)$$

where $\operatorname{sgn}(\cdot)$ is the signum function; q is the pinching initiation parameter; $Z_{j,u}$ is the ultimate value of Z_j given by

$$Z_{j,u} = \frac{A}{(1 + \delta_v \varepsilon_j)(\beta + \gamma)}; \quad (42)$$

$$\zeta_1(\varepsilon_j) = \zeta_s \left[1 - e^{(-p\varepsilon_j)} \right]; \quad (43)$$

and

$$\zeta_2(\varepsilon_j) = (\psi + \delta_\psi \varepsilon_j)(\lambda + \zeta_1), \quad (44)$$

where ζ_s is the measure of total slip; p is the parameter of pinching slope; ψ represents the pinching magnitude; δ_ψ denotes the pinching rate; λ is the parameter of pinching severity/rate interaction.

In Eq. (34), $\xi_t(t)$ is the excitation modeled by the IPSD function (Genovese & Sofi 2023) as

$$S(\omega) = \sigma^2 \beta_0^I \left(\frac{\omega^2}{\omega^2 + (\omega_H^I)^2} \right) \left(\frac{(\omega_L^I)^2}{\omega^4 + (\omega_L^I)^4} \right) \frac{\rho_0}{\pi} \left(\frac{1}{\rho_0^2 + (\omega + \Omega_0^I)^2} + \frac{1}{\rho_0^2 + (\omega - \Omega_0^I)^2} \right), \quad (45)$$

where β_0^I is defined so that the interval stochastic process $\xi_I(t)$ has variance σ^2 ; $\omega_L^I = \Omega_0^I + 0.8\rho_0$, $\omega_H^I = 0.1\Omega_0^I$, and Ω_0^I is the interval predominant circular frequency, ρ_0 is the frequency bandwidth.

In this numerical example, $[m_1, m_2, \dots, m_{10}] = [2.6, 2.6, \dots, 2.6] (\times 10^5 \text{ kg})$, $[k_1, k_2, \dots, k_{10}] = [4.9, 2, 2, 2, 1.8, 1.8, 1.8, 1, 1, 1] (\times 10^7 \text{ N/m})$, the damping ratio $\zeta = 0.05$, and $\mathbf{B} = [1, 1, \dots, 1]^T (\text{kg})$. The other parameters associated with the restoring force [Eq. (38)] and the Bouc-Wen model are given in Table 1. $\theta_1, \theta_2, \dots, \theta_{20}$ are independently distributed, in which $\theta_1, \theta_2, \dots, \theta_{10}$ follow the uniform distribution $U(0.7, 1.3)$ and $\theta_{11}, \theta_{12}, \dots, \theta_{20}$ follow the lognormal distribution with mean equals to 1 and coefficient of variation equals to 0.15. Parameters for the interval excitation are taken as $\sigma^2 = 1.06 (\text{m}^2/\text{s}^4)$, $\rho_0 = 17.33 (\text{rad/s})$, and Ω_0 is bounded within $[23.91, 45.22]$. The response quantity of interest is the maximum displacement of the first DOF, i.e.,

$$X_{\max} = \max(|X_1(t)|), \text{ for } t \in [0, T], \quad (46)$$

where $T = 10$.

Table 1. Values of parameters of Bouc-Wen model

Parameter	ε	A	β	γ	δ_v	δ_η
Value	0.04	1	15	150	1000	1000
Parameter	q	p	δ_ψ	λ	ζ_s	ψ
Value	0.25	1000	5	0.5	0.99	0.05

The double-loop MCS (DL-MCS) is employed to validate the efficiency and accuracy of the proposed method. Notably, the problem involves only one independent epistemic parameter Ω_0 . Therefore, in the outer loop of DL-MCS, 201 uniformly distributed points are selected to perform an exhaustive search across the interval

$[23.91, 45.22]$. Within each inner loop, 10,000 samples are utilized for propagating the aleatory uncertainty. In both the DL-MCS and the proposed decoupled M-PDEM scheme, the excitations are generated using the spectral representation method (Shinozuka 1971). Consequently, additional random phase angles are introduced, significantly raising the overall dimension of the random variables involved to over 1,000. Thus, in the decoupled M-PDEM solution, the MCS samples are directly applied, with each sample assigned an equal probability as $1/N$.

Fig. 3 compares the results obtained by DL-MCS and the proposed decoupled M-PDEM scheme, with 2,000 samples utilized in the decoupled M-PDEM solution. Although a satisfactory agreement between the two results is observed, the accuracy of the decoupled M-PDEM is somewhat reduced compared to the previous example, despite the high sample size. This reduction likely arises from the significantly increased nonlinearity of the current problem, and also the much higher dimensionality of the random parameters involved, which hinders the precise determination of the probabilities assigned to each sample. Nevertheless, the decoupled M-PDEM scheme demonstrates substantially improved computational efficiency compared to the DL-MCS.

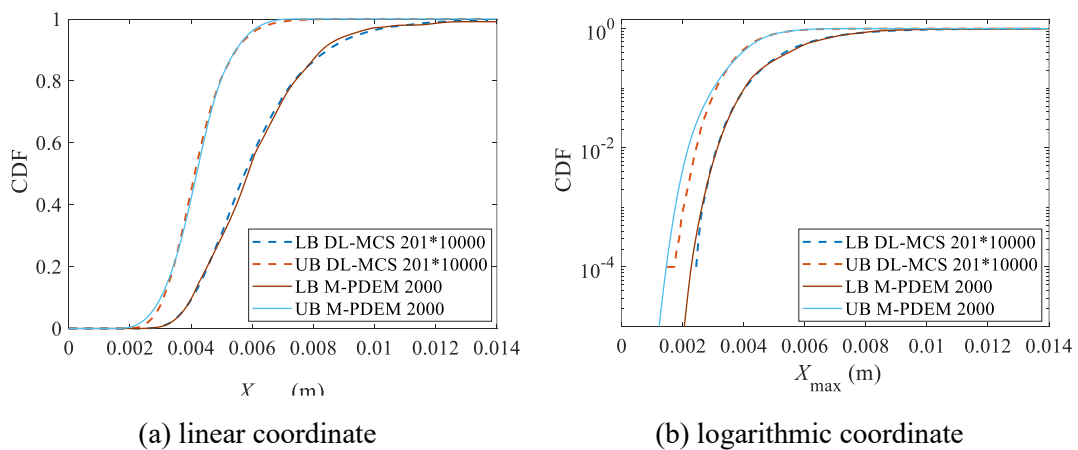


Fig. 3 Upper bounds (UB) and lower bounds (LB) of the CDF of X_{\max} obtained by DL-MCS and the proposed decoupled M-PDEM solution

4.3 Crash-box

Consider a crash box example as illustrated in Fig. 4, which simulates the process of a moving planar impacts on the crash box component. The output of interest is the final internal energy. As a representative benchmark case, the detailed model information is available in Reid (1998), and the analyses are conducted using the CAE Simulation Data Management Systems SCALE.sdm (<https://www.scale.eu/en/products/scale-sdm/>).

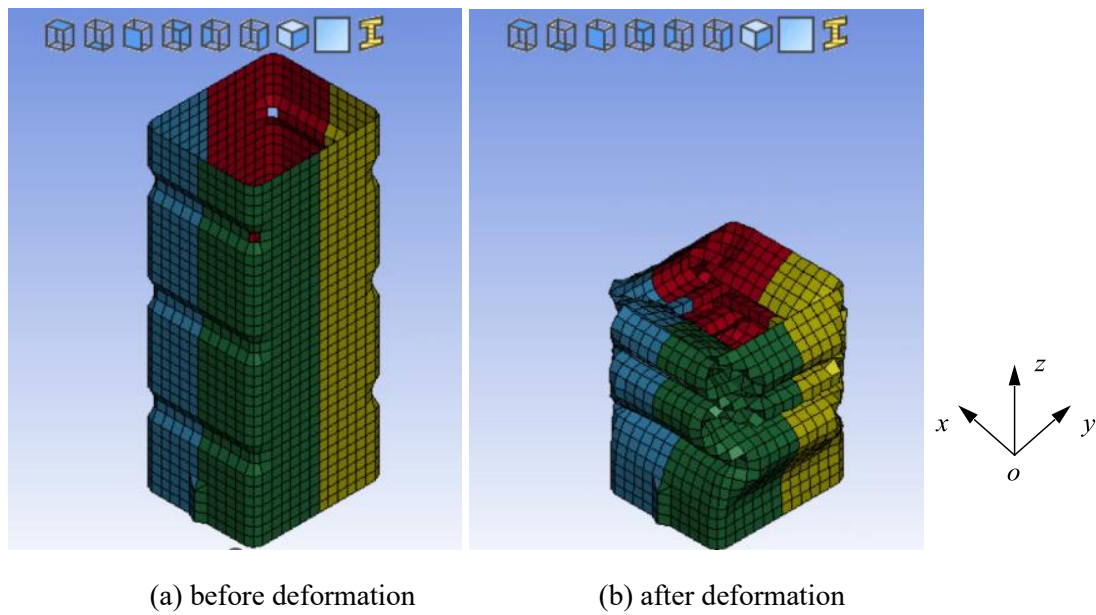


Fig. 4 Schematic diagram of the crash box

The model includes five random input variables and two interval input variables, as listed in Table 2, with parameter values referenced from Hunkeler et al. (2013). The mass and velocity of the impactor were treated as primary epistemic inputs, and thus the assigned uncertainties to these two parameters are expanded to consider a broader range of load cases.

Table 2. Uncertainty input parameters for crash box example

Variable	Description	Uncertainty model
S_x	dimensional scale factor in x direction	$N(1,1/60)$
S_y	dimensional scale factor in y direction	$N(1,1/60)$

τ	scale factor of the thickness of the tube	$N(1, 0.03286)$
α_x	offset of the attack angle in x direction	$U(-1^\circ, 1^\circ)$
α_y	offset of the attack angle in y direction	$U(-1^\circ, 1^\circ)$
M_I	mass of the planar impactor	$[-650, 950]$ (kg)
v_I	velocity of the planar impactor	$[7, 11]$ (m/s)

$N(\mu, \sigma)$ denotes Gaussian distribution with mean equals to μ , and standard deviation equals to σ ; $U(a, b)$ denotes uniform distribution between a and b ; and $[a, b]$ denotes the interval variable with the given bounds.

Due to the prohibitive computational cost of this model, the DL-MCS approach is infeasible. Moreover, given the relatively clear monotonic relationship, where larger M_I and v_I typically lead to higher internal energy, the Vertex MCS method is adopted for validation. This method evaluates the maximum and minimum values of both interval inputs, yielding a total of $2 \times 1000 = 2000$ samples.

Fig. 5 compares the p-box boundaries of the output obtained via the proposed decoupled M-PDEM scheme (with 200 representative analyses) and the Vertex MCS results. Since only 1,000 samples are used for Vertex MCS, the results on logarithmic coordinate are not shown. The proposed solution successfully envelops the Vertex MCS bounds, though the latter produces slightly tighter boundaries. This confirms the reliability of the decoupled M-PDEM solution, as the Vertex MCS results are always equal to or tighter than the true CDF bounds. To further verify the accuracy, the conditional CDFs obtained by the decoupled M-PDEM at the interval vertices are also plotted, showing close agreement with the Vertex MCS results. This demonstrates the accuracy of the proposed procedure.

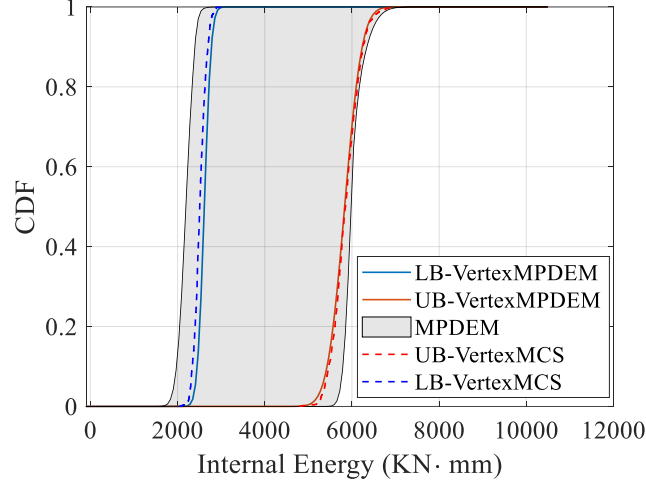


Fig. 5 Comparison of the decoupled M-PDEM results with Vertex MCS results of the crash box example

5 Concluding Remarks

In this work, a unified framework for hybrid aleatory-epistemic uncertainty propagation in dynamical systems has been developed based on the decoupled multi-probability density evolution method (M-PDEM). The proposed framework leverages an augmented random space representation, allowing for the decoupled treatment of various forms of epistemic uncertainty including distribution-free p-boxes. This transforms the hybrid uncertainty propagation problem into a unified task of solving conditional probability distributions, which is efficiently addressed using the decoupled M-PDEM. The framework's effectiveness and versatility have been demonstrated through various numerical examples involving diverse types of uncertain inputs. The proposed approach not only provides an efficient tool for the propagation of hybrid uncertainty in complex dynamical systems, but also constitutes a significant extension of the PDEM methodology.

Despite these advancements, current results highlight opportunities for further improvement, particularly in enhancing the accuracy of the decoupled M-PDEM solution. First, while the approach performs efficiently with one or two epistemic parameters, its extension to higher-dimensional epistemic uncertainty remains

challenging due to the limited number of samples affordable. Second, in reliability analysis where rare events are critical, refinements are needed to capture tail behavior accurately. These limitations could be effectively addressed by integrating advanced sampling techniques and surrogate models in future developments.

Acknowledgement

The authors are grateful for the support by the European Union's Horizon 2020 research and innovation programme under Marie Skłodowska-Curie project GREYDIENT – Grant Agreement n°955393, the German Research Foundation (DFG) (Grant No. FR 4442/2-1) and the National Natural Science Foundation of China (Grant No. 12302037). The authors also highly appreciate SCALE GmbH team for their support in the completion of the crash box example. The discussions and suggestions of Prof. Jian-Bing Chen from Tongji University is highly appreciated.

References

- [1] [Ang AHS, Tang WHC, 1984](#). Probability Concepts in Engineering Planning and Design. Volume II: Decision, Risk, and Reliability [M]. John Wiley & Sons, Singapore.
- [2] [Ang AHS, Tang WHC, 2006](#). Probability Concepts in Engineering Planning and Design [M]. 2nd Edn. John Wiley & Sons, New York, USA.
- [3] [Beer M, Ferson S, Kreinovich V, 2013](#). Imprecise probabilities in engineering analyses [J]. Mechanical Systems & Signal Processing, 37 (1-2): 4-29.
- [4] [Behrendt M, De Angelis M, Comerford L, Zhang YJ, Beer M, 2022](#). Projecting interval uncertainty through the discrete Fourier transform: An application to time signals with poor precision [J]. Mechanical Systems & Signal Processing, 172: 108920.
- [5] [Behrendt M, Lyu MZ, Luo Y, Chen JB, Beer M, 2024](#). Failure probability estimation of dynamic systems employing relaxed power spectral density functions with dependent frequency modeling and sampling [J]. Probabilistic Engineering Mechanics, 75: 103592.

- [6] [Bi SF, Broggi M, Wei PF, Beer M, 2019](#). The Bhattacharyya distance: Enriching the P-box in stochastic sensitivity analysis [J]. *Mechanical Systems & Signal Processing*, 129: 265-281.
- [7] [Bittner M, Broggi M, Beer M, 2024](#). Efficient reliability analysis of stochastic dynamic first-passage problems by probability density evolution analysis with subset supported point selection [J]. *Engineering Structures*. 1;312:118210.
- [8] [Chen JB, Li J, 2007](#). The extreme value distribution and dynamic reliability analysis of nonlinear stochastic structures [J]. *Probabilistic Engineering Mechanics*, 22 (3): 288-296.
- [9] [Chen J, Zhang S, 2013](#). Improving point selection in cubature by a new discrepancy. *SIAM Journal on Scientific Computing* [J]. 35(5):A2121-49.
- [10] [Chen JB, Wan ZQ, 2019](#). A compatible probabilistic framework for quantification of simultaneous aleatory and epistemic uncertainty of basic parameters of structures by synthesizing the change of measure and change of random variables [J]. *Structural Safety*, 78: 76-87.
- [11] [Der Kiureghian A, Ditlevsen O, 2009](#). Aleatory or epistemic? Does it matter? [J]. *Structural Safety*, 31 (2): 105-112.
- [12] [Ditlevsen O, 1982](#). Model uncertainty in structural reliability [J]. *Structural Safety*, 1: 73-86.
- [13] [Faes MGR, Moens D, 2020](#). Recent trends in the modeling and quantification of non-probabilistic uncertainty [J]. *Archives of Computational Methods in Engineering*, 27: 633-671.
- [14] [Faes MGR, Daub M, Marelli S, Patelli E, Beer M, 2021](#). Engineering analysis with probability boxes: A review on computational methods [J]. *Structural Safety*, 93: 102092.
- [15] [Ferson S, Kreinovich V, Ginzburg L, Myers DS, Sentz K, 2003](#). Constructing Probability Boxes and Dempster-Shafer Structures [R]. Sandia National Laboratories, USA.
- [16] [Gao W, Song CM, Tin-Loi F, 2010](#). Probabilistic interval analysis for structures with uncertainty [J]. *Structural Safety*, 32 (3): 191-199.
- [17] [Genovese F, Sofi A, 2023](#). Stochastic analysis of double-skin façades subjected to imprecise seismic excitation. *Materials Research Proceedings*, 26: 555-560.
- [18] [Helton JC, Johnson JD, Oberkampf WL, Sallaberry CJ, 2010](#). Representation of analysis results involving aleatory and epistemic uncertainty [J]. *International Journal of General Systems*, 39 (6): 605-646.
- [19] [Hunkeler S, Duddeck F, Rayamajhi M, Zimmer H, 2013](#). Shape optimisation for crashworthiness followed by a robustness analysis with respect to shape variables: example of a front rail [J]. *Structural and Multidisciplinary Optimization*, 48:367-78.
- [20] [Jerez DJ, Fragkoulis VC, Ni P, Mitseas IP, Valdebenito MA, Faes MG, Beer M, 2024](#). Operator norm-based determination of failure probability of nonlinear oscillators with fractional derivative elements subject to imprecise stationary Gaussian loads. *Mechanical Systems and Signal Processing* [J]. 208:111043.

- [21] Jiang C, Zhang Z, Han X, Liu J, 2013. A novel evidence-theory-based reliability analysis method for structures with epistemic uncertainty [J]. *Computers & Structures*, 129: 1-12.
- [22] Jiang C, Zhang QF, Han X, Liu J, Hu DA, 2015. Multidimensional parallelepiped model - A new type of non-probabilistic convex model for structural uncertainty analysis [J]. *International Journal for Numerical Methods in Engineering*, 103: 31-59.
- [23] Jiang C, Zheng J, Han X, 2018. Probability-interval hybrid uncertainty analysis for structures with both aleatory and epistemic uncertainties: A review [J]. *Structural & Multidisciplinary Optimization*, 57: 2485-2502.
- [24] Li, J, 1996. *Stochastic Structural Systems: Analysis and Modeling* [M]. Science Press, Beijing (in Chinese).
- [25] Li J, Chen JB, 2004. Probability density evolution method for dynamic response analysis of structures with uncertain parameters. *Computational Mechanics* [J]. 34(5):400-9.
- [26] Li J, Chen JB, 2008. The principle of preservation of probability and the probability density evolution equation [J]. *Structural Safety*, 30 (1): 65-77.
- [27] Li J, Chen JB, 2009. *Stochastic Dynamics of Structure* [M]. John Wiley & Sons, Singapore.
- [28] Lind NC, 1983. Models of human error in structural reliability [J]. *Structural Safety*, 1 (3): 167-175.
- [29] Liu HB, Jiang C, Jia XY, Long XY, Zhang Z, Guan FJ, 2018. A new uncertainty propagation method for problems with parameterized probability-boxes [J]. *Reliability Engineering & System Safety*, 172: 64-73.
- [30] Luo Y, Chen JB, Spanos PD, 2022. Determination of monopile offshore structure response to stochastic wave loads via analog filter approximation and GV-GDEE procedure [J]. *Probabilistic Engineering Mechanics*, 67: 103197.
- [31] Lyu MZ, Chen JB, Shen JX, 2024a. Refined probabilistic response and seismic reliability evaluation of high-rise reinforced concrete structures via physically driven dimension-reduced probability density evolution equation [J]. *Acta Mechanica*, 235: 1535-1561.
- [32] Lyu MZ, Fei ZJ, Feng DC, 2024b. Vine-copula-based multi-dimensional fragility analysis of nuclear power plant under sequential earthquakes [J]. *Structural Safety*, 110: 102494.
- [33] Lyu MZ, Feng DC, Cao XY, Beer M, 2024c. A full-probabilistic cloud analysis for structural seismic fragility via decoupled M-PDEM [J]. *Earthquake Engineering & Structural Dynamics*, 53 (5): 1863-1881.
- [34] Lyu MZ, Feng DC, Chen JB, Li J, 2024d. A decoupled approach for determination of the joint probability density function of a high-dimensional nonlinear stochastic dynamical system via the probability density evolution method [J]. *Computer Methods in Applied Mechanics & Engineering*, 418: 116443.

- [35] [Lyu MZ, Liu YY, Chen JB, 2025a](#). A novel model and simulation method for multivariate Gaussian fields involving nonlinear probabilistic dependencies and different variable-wise spatial variabilities [J]. *Reliability Engineering & System Safety*, 260: 110963.
- [36] [Lyu MZ, Yang JS, Chen JB, Li J, 2025b](#). High-efficient non-iterative reliability-based design optimization based on the design space virtually conditionalized reliability evaluation method [J]. *Reliability Engineering & System Safety*, 254: 110646.
- [37] [Ma F, Zhang H, Bockstedte A, Foliente GC, Paevere P, 2004](#). Parameter analysis of the differential model of hysteresis. *J. Appl. Mech.* [J].71(3):342-9.
- [38] [Moens D, Vandepitte D, 2005](#). A survey of non-probabilistic uncertainty treatment in finite element analysis [J]. *Computer Methods in Applied Mechanics & Engineering*, 194 (12-16): 1527-1555.
- [39] [Möller B, Beer M, 2004](#). *Fuzzy Randomness: Uncertainty in Civil Engineering and Computational Mechanics* [M]. Springer Science & Business Media, New York, USA.
- [40] [Moore RE, Kearfott RB, Cloud MJ, 2009](#). *Introduction to Interval Analysis* [M]. SIAM.
- [41] [Ni BY, Jiang C, 2020](#). Interval field model and interval finite element analysis [J]. *Computer Methods in Applied Mechanics & Engineering*, 360: 112713.
- [42] [Ni P, Jerez DJ, Fragkoulis VC, Faes MG, Valdebenito MA, Beer M, 2022](#). Operator norm-based statistical linearization to bound the first excursion probability of nonlinear structures subjected to imprecise stochastic loading. *ASCE-ASME Journal of Risk and Uncertainty in Engineering Systems, Part A: Civil Engineering* [J]. 8(1):04021086.
- [43] [Papadimitriou C, 2004](#). Optimal sensor placement methodology for parametric identification of structural systems [J]. *Journal of Sound & Vibration*, 278 (4-5): 923-947.
- [44] [Reid JD, 1998](#). *LS-DYNA examples manual*. Livermore Software Technology [R]. CA, USA.
- [45] [Sankararaman S, Mahadevan S, 2011](#). Likelihood-based representation of epistemic uncertainty due to sparse point data and/or interval data [J]. *Reliability Engineering & System Safety*, 96 (7): 814-824.
- [46] [Sankararaman S, Mahadevan S, 2013](#). Separating the contributions of variability and parameter uncertainty in probability distributions [J]. *Reliability Engineering & System Safety*, 112: 187-199.
- [47] [Shinozuka M, 1971](#). Simulation of multivariate and multidimensional random processes[J]. *The Journal of the Acoustical Society of America*, 49(1B):357-68.
- [48] [Soize C, 2000](#). A nonparametric model of random uncertainties for reduced matrix models in structural dynamics [J]. *Probabilistic Engineering Mechanics*, 15 (3): 277-294.
- [49] [Soize C, 2017](#). *Uncertainty Quantification: An Accelerated Course with Advanced Applications in Computational Engineering* [M]. Springer.

- [50] [Tao JJ, Chen JB, 2022](#). A hierarchy model for the uncertainty quantification of spatial variability in the constitutive parameters of concrete in structures [J]. *Structural Safety*, 95: 102181.
- [51] [Toussi S, Yao JTP, 1982](#). Assessment of structural damage using the theory of evidence [J]. *Structural Safety*, 1 (2): 107-121.
- [52] [Wan ZQ, Chen JB, Li J, Ang AHS, 2020](#). An efficient new PDEM-COM based approach for time-variant reliability assessment of structures with monotonically deteriorating materials [J]. *Structural Safety*, 82: 101878.
- [53] [Wan ZQ, Hong X, Tao WF, 2023](#). Improvements to the probability density evolution method integrated with the change of probability measure on quantifying hybrid uncertainties [J]. *Structural Safety*, 103: 102342.
- [54] [Wan ZQ, Tao WF, Wang XL, Gao Y, 2024](#). Propagation of hybrid uncertainty by synthesizing B-spline chaos and augmented change of probability measure [J]. *Structural Safety*, 111: 102524.
- [55] [Wan ZQ, Lyu MZ, Hong X, Song YP, Chen JB, Ghanem R, 2025](#). Joint probabilistic modelling and sampling from small data via probabilistic learning on manifolds and decoupled multi-probability density evolution method [J]. *Probabilistic Engineering Mechanics*, 79: 103736.
- [56] [Wang GY, Qiao Z, 1993](#). Linear programming with fuzzy random variable coefficients [J]. *Fuzzy Sets & Systems*, 57 (3): 295-311.
- [57] [Wang ZH, Ghanem R, 2021](#). An extended polynomial chaos expansion for PDF characterization and variation with aleatory and epistemic uncertainties [J]. *Computer Methods in Applied Mechanics & Engineering*, 382: 113854.
- [58] [Wang D, Sun W, Li J, 2021](#). An RKPM-based formulation of the generalized probability density evolution equation for stochastic dynamic systems. *Probabilistic Engineering Mechanics* [J]. 66:103152.
- [59] [Wang ZW, Lu XF, Zhang WM, Fragkoulis VC, Zhang YF, Beer M, 2024](#). Deep learning-based prediction of wind-induced lateral displacement response of suspension bridge decks for structural health monitoring [J]. *Journal of Wind Engineering & Industrial Aerodynamics*, 247: 105679.
- [60] [Wei P, Lu Z, Song J, 2014](#). Extended Monte Carlo simulation for parametric global sensitivity analysis and optimization. *AIAA journal* [J]. 52(4):867-78.
- [61] [Wei PF, Song JW, Bi SF, Broggi M, Beer M, Lu ZZ, Yue ZF, 2019a](#). Non-intrusive stochastic analysis with parameterized imprecise probability models: I. Performance estimation [J]. *Mechanical Systems & Signal Processing*, 124: 349-368.
- [62] [Wei PF, Song JW, Bi SF, Broggi M, Beer M, Lu ZZ, Yue ZF, 2019b](#). Non-intrusive stochastic analysis with parameterized imprecise probability models: II. Reliability and rare events analysis [J]. *Mechanical Systems & Signal Processing*, 126: 227-247.
- [63] [Xiang MJ, Lyu MZ, Shen JX, Xu ZK, Chen J, 2025](#). System reliability analysis of building clusters considering inter-structural seismic demand correlation [J]. *Structural Safety*, 112: 102528.

- [64] [Xiu DB, 2010](#). Numerical Methods for Stochastic Computations: A Spectral Method Approach [M]. Princeton University Press.
- [65] [Yang JS, Wan ZQ, Jensen HA, 2025](#). An efficient strategy for information reuse in probability density evolution method considering large shift of distributions with multiple random variables [J]. Probabilistic Engineering Mechanics, 79: 103728.
- [66] [Yao JTP, Furuta H, 1986](#). Probabilistic treatment of fuzzy events in civil engineering [J]. Probabilistic Engineering Mechanics, 1 (1): 58-64.
- [67] [Zadeh LA, 1965](#). Fuzzy Sets [J]. Information & Control, 8 (3): 338-353.
- [68] [Zhou T, Peng Y, Li J, 2019](#). An efficient reliability method combining adaptive global metamodel and probability density evolution method [J]. Mechanical Systems and Signal Processing. 131:592-616.